

# Passive Shim Design and a Shimming Approach for Biplanar Permanent Magnetic Resonance Imaging Magnets

Hector Sanchez Lopez, Feng Liu, Ewald Weber, and Stuart Crozier

School of Information Technology and Electrical Engineering, University of Queensland, St. Lucia, Brisbane Qld 4072, Australia

**This paper presents a new passive shim design method and a novel shimming procedure to correct the magnetic field inhomogeneities generated by C-shape permanent biplanar magnetic resonance imaging magnets. The method expresses the shim distribution as a sum of orthogonal functions multiplied by unknown amplitudes. The oscillating modes of the shim magnetization-thickness function are normalized within a finite disk. By minimizing the shim set weight and constraining the magnetization-thickness function, the method produces a continuous map of the required shim contribution. The map defines the shim shape and a discrete process then determines the regions where no shim contributions are needed. With this methodology, passive shims capable of generating magnetic field harmonics with minimal impurities and ferro-shim pieces can be generated. The paper reports a study of magnetic coupling among the iron pieces and its influence over the magnetic field harmonics of linear and nonlinear iron, and demonstrates that the exclusion of the magnetic coupling in the shimming process produces an unacceptable error in the final shimmed field homogeneity. The proper selection and arrangement of individual shim sizes produces a better conditioned field source matrix and hence improves the design. A number of examples show that the new method can effectively cancel target impurity harmonics while controlling high-order harmonics.**

*Index Terms*—Magnetic resonance imaging (MRI), passive shim, passive shimming, zonal and tesseral harmonics.

## I. INTRODUCTION

**M**AGNETIC RESONANCE IMAGING (MRI) has been successfully used as a noninvasive diagnostic tool for imaging soft tissue. The patient is placed within a strong and very homogenous magnetic field (a few parts per million) in the imaging region, also known as the diameter of the spherical volume (DSV), to align the magnetic moments of (usually) protons in water molecules. A separate gradient coil set generates a strong and linear magnetic field in the DSV to decode the MR signal in the time and frequency domains in order to form an MR image. The radio-frequency (RF) coil transmits RF energy and receives the MR signal response.

MRI for clinical purposes has often been performed with horizontal magnets where the patient lies along the axial axis; however, this kind of structure produces a tunnel effect causing some patients to experience claustrophobia during a scan [1]. Using lower field, open-type magnet structures for MRI experiments, can minimize the claustrophobic effects and at the same time offer some interaction between the medical attendant and the patient. However, in the open-type structure low field is generated and hence images of inferior quality are obtained when compared to those obtained at high magnetic fields using superconducting magnets. The C-shape open configuration is one of the commonly used open-type structures where the patient is placed between planar poles pieces. The pole pieces are attached, generally, to a permanent magnet and then joined to a iron yoke forming a C-shape like form [2], [3]. New research involving symmetric and asymmetric completely open structures are still in progress [4]–[6].

It is known, that due to machining tolerances during manufacturing, unavoidable errors are introduced in the expected

magnetic field homogeneity and as a consequence, a passive and/or active correction process is required to bring the homogeneity to within clinical MRI requirements. The magnetic field induction satisfies Laplace's equation in regions in the absence of currents and magnetic field sources; hence, the vector potential can be expressed in terms of spherical harmonics. As a consequence, the field impurities can be represented in that basis set and an active or/and passive source of magnetic field is tailored conveniently around the DSV to cancel the undesired harmonics.

Several analytical and numerical techniques for designing active and passive shim have been presented [7]–[14]; where a number of workers have focused on biplanar active shim designs [8], [9], [15]. However, very little work concerning biplanar passive shimming has been published.

The passive shimming process generally arranges small pieces of ferromagnetic material in a convenient way so as to produce the same amplitude but opposite sign of the contaminant harmonics [11], [13], [14], [16], [17]. In permanent magnet design, low order harmonic impurities often remain in the expected magnetic field and hence a first coarse shimming is performed by reshaping the pole faces attached to the biplanar permanent magnet [18]–[21]. Usually at a later stage small pieces of magnetic materials (iron/permanent magnets) are attached to the pole face for a fine tuning of the target field homogeneity [22]–[24]. Existing methods have been limited to the use of an optimization algorithm to cancel a set of magnetic field harmonics and to minimize the volume of an array of ferroshim pieces [25]. In all of these cases, the iron pieces have a predefined and fixed shape; moreover, there is unclear definition about the optimal radial domain size for a shim array to cancel a set of harmonics.

In this research, we expressed the magnetization-thickness function in terms of a series of orthogonal azimuthal and radial, sinusoidal and cosinusoidal harmonics. By minimizing the shim set weight, under linear constraints of the target harmonics and constraining the maximal and minimal magnetization-thickness value, the method produces a continuous map of the shim

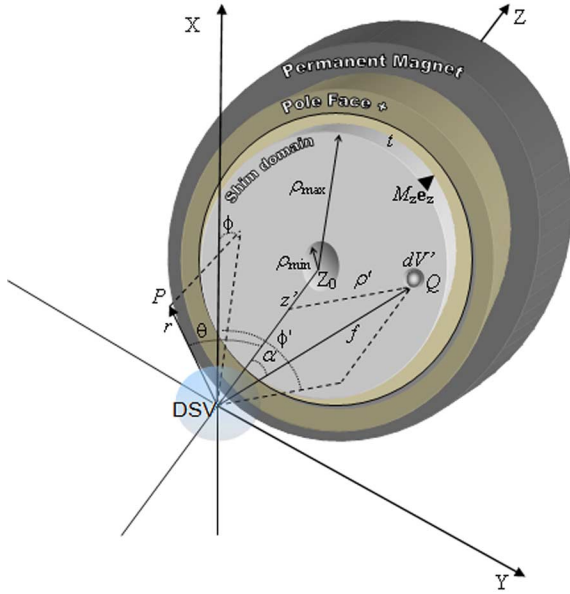


Fig. 1. Coordinate system used in the shimming procedure. Only one half of the shim, pole face, and permanent magnet devices are shown.  $\rho_{\min}$  is the minimal internal radius of the magnetized disk. The light shadow sphere centered at  $(0,0,0)$  represents the DSV region.

topology defining the shim shape and magnetization-thickness strength. If the same material with only one direction (positive) magnetization is used, then iron pieces of thickness unit can be placed in the positive domain of map and thereafter a linear programming (LP) algorithm can be applied to find the discrete thickness distribution that generates the target harmonics. The matrix that contains the shim contribution to the magnetic field harmonics is better conditioned and superior solutions are obtained as a result.

In the discrete shim array the magnetic coupling among shim pieces has been taken into account for an accurate thickness calculation. Both linear and nonlinear iron cases are studied and the impact of neglecting the magnetic coupling over the final shimmed homogeneity is also analyzed. An optimal combination of shim sizes for cancelling low order and controlling high order with a minimum rounding impact over the shimmed homogeneity is presented. We then present a set of passive shim profiles to produce zonal and tesseral harmonics of high purity. The algorithm is tested with a simulated example for shimming a set of harmonics.

## II. MATERIALS AND METHODS

### A. Magnetic Field Spherical Harmonics

Let us assume an isotropic, linear, nonhysteresis, ferromagnetic disk of radius  $\rho_{\max}$ , uniformly magnetized ( $M_z \mathbf{e}_z$ ) along the axial axis. See Fig. 1. The disk thickness  $t$  is much smaller than the axial distance ( $2Z_0$ ) between the two pole faces and thick enough to produce an induced magnetization  $M_z$  along the axial axis. We consider the disk immersed in a magnetizing field  $H_z(\rho', \phi') \mathbf{e}_z$ . We assume no magnetization is induced along the radial and azimuthal direction. The axial component of the magnetic field induction at the point  $P(r, \theta, \phi)$  due to a magnetized

element of volume  $dV' = tdA'$  located at the point  $Q(f, \alpha, \phi')$  can be written as [7]

$$dB_z = \frac{\mu_0 M_z t dA'}{4\pi} \sum_{n=0}^{\infty} \sum_{m=0}^n \varepsilon_m \frac{(n-m+2)!}{(n+m)!} P_{n+2}^m(\cos \alpha) h_{f, \text{fill}} \times \frac{r^n}{f^{n+3}} P_n^m(\cos \theta) \cos m(\phi - \phi') \quad (1)$$

where the Neumann factor  $\varepsilon_m = 1$  if  $m = 0$ ; otherwise  $\varepsilon_m = 2$

$$f = \sqrt{\rho'^2 + Z_0^2} \quad \text{and} \quad \cos \alpha = \frac{Z_0}{f}. \quad (2)$$

$P_n^m$  is the associated Legendre function of order  $n$  and degree  $m$ . We define the element  $dA'$  as

$$dA' = \rho' \cdot d\rho' d\phi'. \quad (3)$$

Equation (1) considers the magnetized element located in one pole face ( $+Z_0$ ). We are only interested in the axial component, in this case, because it is the dominant component produced by the MRI main magnet in the DSV.

Assuming a negligible magnetic coupling among the magnetized elements in the continuous shim domain and pole faces we can write the magnetization-thickness function as

$$S(\rho', \phi') = t \cdot M_z(\rho', \phi') \quad (4)$$

where

$$M_z(\rho', \phi') = \sum_{n'=1}^N \sum_{m'=0}^M (a_{m'} \cos m' \phi' + b_{m'} \sin m' \phi') \times (c_{n'} \cos K_{n'}(\rho' - \rho_{\min}) d_{n'} \sin K_{n'}(\rho' - \rho_{\min})); \quad \rho_{\min} \leq \rho' \leq \rho_{\max}.$$

The scalar magnitude  $S(\rho', \phi')$  represents magnetization-thickness strength at the point  $(\rho', \phi')$ . The function is applied to each pole face and is defined and different from zero only within the disk domains.

The parameters  $(a_{m'}, b_{m'})$  and  $(c_{n'}, d_{n'})$  represent the unknown amplitudes of the oscillating modes of shim magnetization-thickness along the azimuthal and radial directions, respectively

$$K_n = \frac{n\pi}{\rho_{\max} - \rho_{\min}}.$$

The parameters  $N$  and  $M$  define the number of modes along the radial and azimuthal direction, respectively.

The assumption of nonmagnetic coupling in the continuous shimming approach simplifies the calculation method and minimizes the computational burden. This simplification permits us to produce a quick definition of the effective discrete shim domain through the continuous magnetization-thickness map for an efficient shimming procedure. However, in the following section, we will see that the magnetic coupling must be taken into

account for an accurate shimming process when using discrete shim pieces.

Under the assumptions mentioned above, and separating the source information from the field spatial dependence in (1), the amplitudes corresponding to the magnetic field oscillating harmonics are written as

$$A_{nm} = \int_{\rho_{\min}}^{\rho_{\max}} \int_0^{2\pi} C_{nm}(\rho', \phi') \cos m\phi' d\rho' d\phi' \quad (5)$$

$$B_{nm} = \int_{\rho_{\min}}^{\rho_{\max}} \int_0^{2\pi} C_{nm}(\rho', \phi') \sin m\phi' d\rho' d\phi' \quad (6)$$

where

$$C_{nm}(\rho', \phi') = \frac{\varepsilon_m \mu_0 (n-m+2)!}{4\pi (n+m)!} \frac{\rho'}{(\rho'^2 + (\pm Z_0)^2)^{\frac{n+3}{2}}} \\ \times \left[ S(\rho', \phi')^U P_{n+2}^m \left( \frac{+Z_0}{\sqrt{\rho'^2 + (+Z_0)^2}} \right) \right. \\ \left. + S(\rho', \phi')^L P_{n+2}^m \left( \frac{-Z_0}{\sqrt{\rho'^2 + (-Z_0)^2}} \right) \right]. \quad (7)$$

The superscripts (U and L) refer to the upper and the lower pole faces. The manner in which (5) and (6) have been expressed allows us to find an optimal magnetization-thickness map to produce a target harmonic for a given disk radial domain, DSV size, and distance between the two pole faces. This map then determines where to place a discrete set of ferrosims to generate, with minimal impurities, a particular harmonic or a combination of harmonics. The harmonic symmetry along the radial and/or azimuthal direction characterizes the shim pattern symmetry through the function  $S(\rho', \phi')$ . For this reason, we have included in  $S(\rho', \phi')$  odd and even functions in order to cover all the possible harmonic symmetries and amplitudes. Special attention is required in defining  $N$  and  $M$  to avoid an over-fitting that can result in high-frequency oscillation of the  $S(\rho', \phi')$  values which appear close to the disk end at ( $\rho' \approx \rho_{\max}$ ). The minimal number of axial  $N$  and azimuthal modes  $M$  that corrects a target inhomogeneous magnetic field can be the criteria that define the optimal  $M$  and  $N$  values.

If the thickness is an *a priori* known variable and its value is much smaller than the pole faces distance and DSV size, then magnetized iron pieces can be placed in the shim domains using the topology defined by  $S(\rho', \phi')$ . An approach for a discrete shim piece was presented in [26], in which the author fixed the piece thicknesses and the magnetization orientation and constrained its value between a maximal and a minimal boundary. The iterative process included in finite-element software for magnetization calculation; a computationally expensive method. Combining this method with (5) and (6), it is possible to calculate the magnetization expressed in the form of (4) as an initial solution and starting point for the shimming process.

The limitation for a practical implementation of the solutions obtained using the present approach is to find proper  $M_z(\rho', \phi')$  values [see (4)] and directions of local magnetizations for a given continuous magnetization-thickness map. However, if ferrosim pieces with a known magnetization  $M_z$  value with only one direction (positive) is used for a given  $S(\rho', \phi')$  map, then

iron pieces of thickness unit can be placed in the positive domain of  $S(\rho', \phi')$ . Thereafter, an LP algorithm can be applied to find the discrete thickness distribution that generates the target field. This implementation can help us find a practical solution.

### B. Passive Shimming Approach

The passive shimming approach is a typical inverse problem. One of the remaining challenges in the inverse problem is how to find practical solutions; the solution depends strongly on the condition of the source matrix. In designing magnetic devices for MRI (shim and gradient coils), we have found that the physical distance between the sources is generally much smaller than the distance between the sources and the DSV surface. Moreover, the magnetic field for active sources (current loops) depends inversely on the distance to the power of three. This means that the magnetic field generated by active sources at the DSV by the unit strength (current) will produce similar values. This effect is the main cause of ill-conditioning in the source matrix. The situation is even more critical for passive shim design that uses the dipole approximation for the iron simulation. The distance depends on the power of five; hence, we expect a highly ill-conditioned matrix for passive shim design. If a conventional shimming method is used, where the passive shim array is set up without an optimal criteria (effective discrete shim domain), and shim elements without any contribution are also considered in the source matrix, then a highly ill-conditioned matrix is produced, making it more difficult to find practical solutions.

Moreover, depending on the sign, amplitude, and symmetry of the target harmonic, there are some regions in the shim domain where the iron pieces are not required. Previous methods have never taken into account these subregions to improve the condition of the source matrix. These effects are explicitly taken into account in the algorithm presented here.

Fig. 2 shows a flowchart of our shimming approach. In this figure,  $A_{nm}^{\text{target}}$  and  $B_{nm}^{\text{target}}$  are the target coefficients determined in a deconvolution of the measured magnetic field over the DSV [27]. After the amplitudes of the harmonics are determined, an optimization algorithm is then used to obtain the amplitudes ( $a_{m'}$ ,  $b_{m'}$ ) and ( $c_{n'}$ ,  $d_{n'}$ ), of the  $S(\rho', \phi')$  function that minimize the disk weight  $W(\rho', \phi')$  and at the same time cancel the target harmonics and controls the high order field components excluded in the target set. The optimization problem can be expressed as

$$\min \sum_{i=1}^{N_\rho} \sum_{j=1}^{N_\phi} W(\rho_i, \phi_j) \\ \text{subject to} \\ -\varepsilon \leq A_{nm} + A_{nm}^{\text{target}} \leq \varepsilon; \\ -\varepsilon \leq B_{nm} + B_{nm}^{\text{target}} \leq \varepsilon; \\ S_{\min} \leq S(\rho_i, \phi_j) \leq S_{\max}; \\ i = 1 \dots N_\rho, j = 1 \dots N_\phi \quad (8)$$

where  $\varepsilon$  is a relaxation factor or relative target homogeneity corresponding to the shimming iteration process.  $N_\rho$  and  $N_\phi$  are the number of discrete radial and azimuthal shim pieces;  $S_{\min}$  and  $S_{\max}$  correspond to the minimal and maximal permissible magnetization-thickness value in the ferro-disk domain.

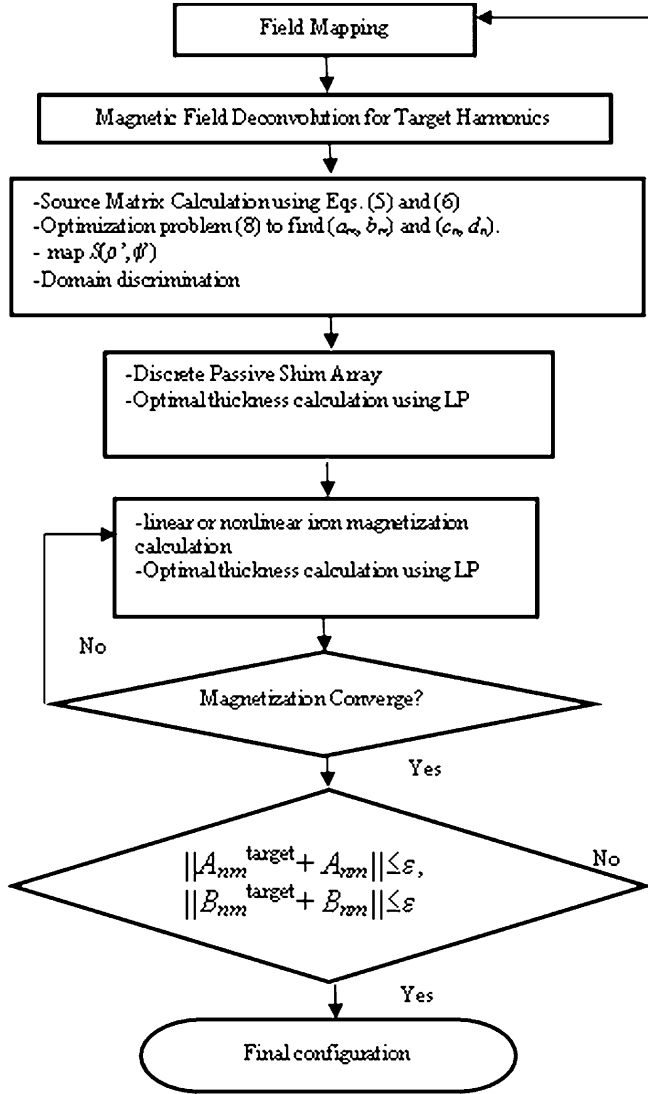


Fig. 2. Passive shimming procedure considering the continuous  $S(\rho', \phi')$  mapping approach for optimal shim solutions. LP: linear programming.

Before the shimming process is achieved, it is useful to perform a simulated shimming approach where the  $S_{\min}$  and  $S_{\max}$  values are selected to guarantee a convergence and potentially meet the target homogeneity. In a practical shimming exercise meeting, the target homogeneity is never assured. It depends on the given DSV, available shim space, and initial unshimmed field homogeneity.

Additional, necessary conditions must be satisfied for the problem (8) to reach a local minimum within the domain defined in (4). The conditions can be written as

$$\frac{\partial W(\rho', \phi')}{\partial \rho'} = \frac{\partial W(\rho', \phi')}{\partial \phi'} = 0 \quad (9)$$

and

$$\frac{\partial^2 W(\rho', \phi')}{\partial \rho' \partial \rho'} = \frac{\partial^2 W(\rho', \phi')}{\partial \phi' \partial \phi'} \geq 0. \quad (10)$$

By assigning zero amplitude to the harmonics excluded in the target set, one can control the generation of undesired impurities. The target harmonic  $A_{00}^{\text{target}}$  is set to zero in order to ensure

a minimum contribution to the main  $B_0$  field strength from the shim set array. The same strategy can be used to control the influence of high order harmonics excluded in the harmonic target set  $(A_{nm}^{\text{target}}, B_{nm}^{\text{target}})$ .

The negative value of  $S(\rho', \phi')$  defines the areas where the discrete shims do not contribute to the shimming process; hence, no shim elements are set in these regions. After the regions with positive  $S(\rho', \phi')$  values are found, discrete pieces of shim are placed and an LP optimization algorithm is then employed to obtain the discrete thickness distribution [13]. At this stage, the thicknesses are calculated neglecting the change of magnetization value due to magnetic coupling. However, we know that this approach is valid only when the iron pieces are saturated or very far from each other. When shimming a horizontal superconducting magnet where the central field is over 1.5 T, in general, the iron used for passive shimming is saturated; therefore, the thickness is calculated without considering magnetic coupling between shims. However, in open-type permanent based MRI magnets, the main field generated is between  $\sim 0.2$  and  $\sim 0.7$  T and both magnetic coupling and iron linearity/nonlinearity have to be taken into account for an accurate thickness calculation. Magnetic coupling is calculated only for iron pieces that appear in the valid domain defined by the thickness map and for ferrosims with nonzero thicknesses. In this way, the matrix that contains the magnetic coupling coefficients is efficiently calculated in a few seconds. Because the main objective of the current approach is to demonstrate the methodology described in Fig. 2, the magnetic coupling between the poles and the shim pieces was not considered. In Section III, the impact over the magnetic field harmonics, with the assumption of non-magnetic coupling among the shim iron pieces for a discrete ferrosim set, will be investigated.

A zero order expansion of the magnetization is used, where this quantity is taken to be uniform within each shim piece, and point collocation for field evaluation [28]. After updating the magnetization at each shim piece with nonzero thickness, an LP algorithm is then employed to update the thickness in each shim piece with nonzero thickness. The process is repeated until no change in magnetization is produced as a result of the change of thickness for the given DSV and target harmonics. See Fig. 2. The magnetic field homogeneity is evaluated after magnetization and thickness calculation. Depending on the final target homogeneity and available space for the iron shim, a decision for the next step is made.

The Matlab software provides a set of optimization procedures capable of handling functions with linear and nonlinear constraints. The *fmincon* algorithm in Matlab was used to solve the problem (8). In order to obtain practical solutions, the *round* procedure from Matlab software was used to produce integer proportions of the minimal shim thickness  $t_0$ .

### III. RESULTS AND DISCUSSIONS

In this section, we applied our method to a series of simulated situations and demonstrate that our algorithm can effectively generate any kind of harmonic with minimal impurities.

In all the simulations, the minimum and maximum disk radius were set to  $\rho_{\min} = 0.025$  m and  $\rho_{\max} = 0.5$  m, respectively.

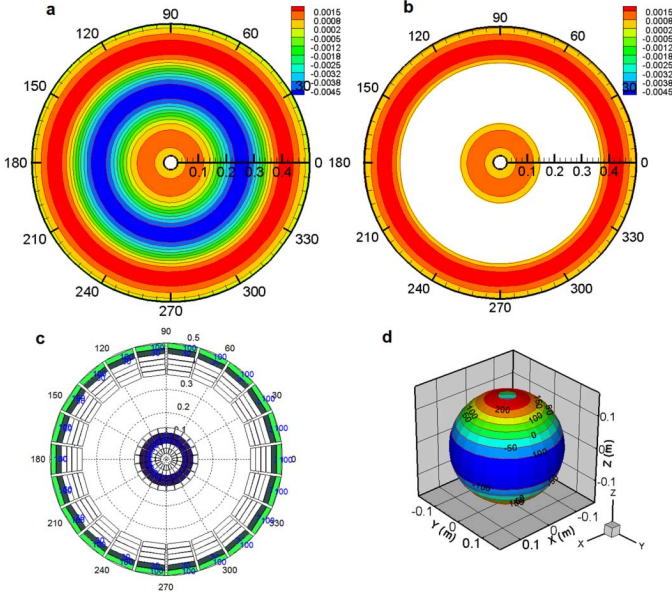


Fig. 3. Continuous magnetization-thickness map ( $S(\rho', \phi') / \max(\|S(\rho', \phi')\|) \cdot t$ ) (a) and the valid domain for the discrete shim array (b). Discrete shim design to generate an  $A_{20}^{\text{target}} = -275$  ppm (c) with iron. The empty space in (b) shows the invalid domain. The magnetic field profile (d) generated by the discrete shim set (c) at the DSV. Units in (a,b) are given in meters and units in (d) are given in micro Tesla.

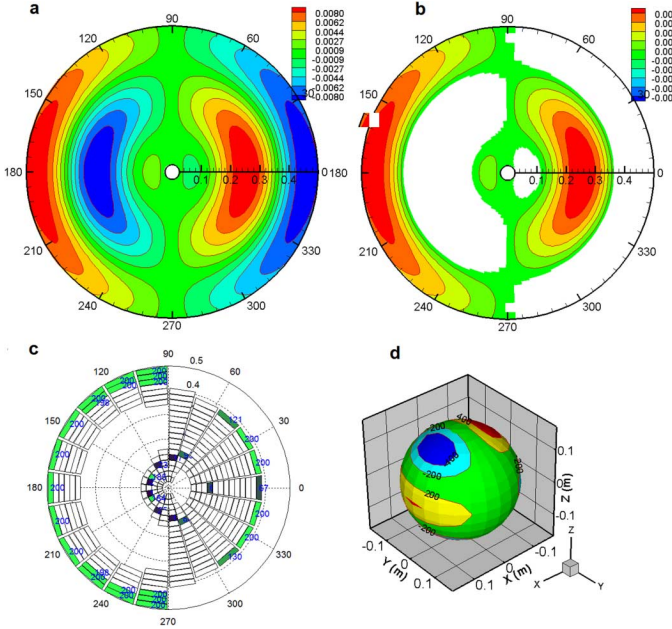


Fig. 4. Continuous magnetization-thickness map ( $S(\rho', \phi') / \max(\|S(\rho', \phi')\|) \cdot t$ ) (a) and the valid domain for the discrete shim array (b). Discrete shim design to generate an  $A_{31}^{\text{target}} = -275$  ppm (c) with iron. The empty space in (b) shows the invalid domain. The magnetic field profile (d) generated by the discrete shim set (c) at the DSV. Units in (a,b) are given in meters and units in (d) are given in micro Tesla.

The DSV size of 31 cm was used ( $r_0 = 15.5$  cm, normalization radius). The distance between the pole face was set to 46 cm ( $Z_0 = 23$  cm). We assume the array of discrete iron pieces immersed in a homogenous magnetizing field of  $H_c e_z = 1500$  (A/m). The relative permeability ( $\mu_r$ ) for the iron shim was set to 1500. We assume that the iron used for the shim pieces is nonhysteresis, linear, and isotropic. For the discrete shim array,

$N_\rho = 21$  and  $N_\phi = 22$  were used for each pole face. A minimum azimuthal and radial gap of 0.5 mm was set between shim pieces. A minimal shim thickness  $t_0 = 0.05$  mm was used for the discrete simulations.

A target of  $\|275\|$  ppm was set for each target harmonic. For comparison between different shim sets, the following figure of merit was used:

$$\eta = \frac{\sum_{n=0}^{N_{\max}} \sum_{m=0}^n \|A_{nm}\| + \sum_{n=0}^{N_{\max}} \sum_{m=0}^n \|B_{nm}\|}{\sum_{i=1}^{N_z} \sum_{j=1}^{N_\phi} W(\rho_i, \phi_j)} \frac{1}{\sigma} \quad (11)$$

where  $N_{\max}$  is the maximum order of minimization,  $\sigma$  is the achieved peak-to-peak magnetic field homogeneity in ppm; the harmonic amplitudes ( $A_{nm}, B_{nm}$ ) contain the contribution of the discrete shim array to each order  $n$  and degree  $m$ . The coefficients are normalized at the radius  $r_0$  and are reported in Tesla. The figure of merit (11) expresses how efficient the discrete shim set is for shimming a given target homogeneity and at the same time characterizes the final magnetic field homogeneity. The expression (11) is only valid for the same specific DSV size, iron disk size, piece iron magnetic property, number of discrete shim array ( $N_\rho \cdot N_\phi$ ), target homogeneity, and unit contribution of all the shim set to the field harmonic amplitudes.

#### A. Generating Zonal and Tesseral Harmonics

In order to generate a second order zonal harmonic, we set all the target harmonics ( $A_{nm}^{\text{target}}$  and  $B_{nm}^{\text{target}}$ ) to zero with the exemption of the  $A_{20}^{\text{target}}$ , which in this example is set to  $-275$  ppm. The number of modes along the radial  $N$  and azimuthal  $M$  direction was set to 3. Fig. 3 shows the resulting continuous domain map and the discrete shim set to generate a second order zonal harmonic. Due to the pattern symmetry with respect to the plane  $Z = 0$ , only upper shim profile has been shown. The white region in Fig. 3(b) is the ineffective domain or the zone where the pieces of shims are not needed (magnetization has reversed direction). The discrete map shows symmetric rings with different thicknesses to compensate the order: zero, four, and six. The symmetry compensates odd orders and no dependency along the azimuthal direction is generated.

The total weight (two pole faces) of the shim profile shown in Fig. 3(c) is 6.31 kg and the final homogeneity was 4.044 ppm. These values produce a figure of merit of  $1.068 \cdot 10^{-5}$  T/(kg  $\cdot$  ppm). The generated harmonic is at least 680 times larger than the remaining harmonics ( $m = 0, n = 0, 4$ , and 6). It is noted that the tesseral harmonic values are zero. The difference between the target and the produced harmonics was only  $-2.21$  ppm. The resulting profile shown in Fig. 3(a) is similar to the pole shape resulting from shimming low order harmonics basically generated by the permanent magnets [18].

If the discrete shim array is uniformly located in the domain ( $\rho', \phi'$ ) using the conventional shimming approach, then  $\eta = 2.08 \cdot 10^{-6}$  T/(kg  $\cdot$  ppm); which is 5 times smaller than the same parameter generated by the shim set shown in Fig. 3(c). The condition number of the source matrix is 8.2 larger than that produced by the new source matrix.

Fig. 4 describes the continuous thickness map and the valid domain to produce  $A_{31}^{\text{target}} = -275$  ppm. The figure of merit of this design was  $\eta = 1.604 \cdot 10^{-5}$  T/(kg  $\cdot$  ppm). The difference between the target and the produced harmonic was only

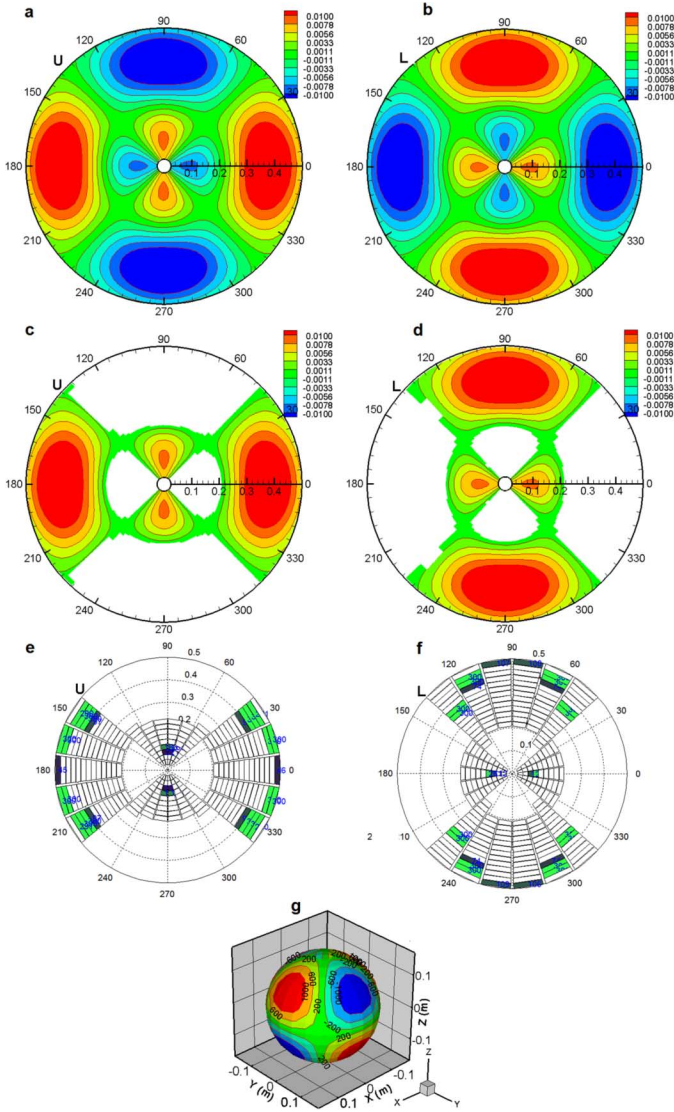


Fig. 5. Continuous magnetization-thickness map  $(S(\rho', \phi')/\max(\|S(\rho', \phi')\|) \cdot t)$  (a and b) and the valid domain for the discrete shim array (c and d). Discrete shim design to generate an  $A_{32}^{\text{target}} = -275$  ppm (e and f) with iron. The empty space in (c and d) shows the invalid domain. The magnetic field profile (g) generated by the discrete shim set (e and f) at the DSV. Units in (g) are given in micro Tesla. Units in (a,b,c,d) are given in meters. The letters (U and L) identify the upper and lower pole faces.

$-0.18$  ppm. The largest remaining harmonics were  $A_{11}$  and  $B_{11}$ . However, the generated  $A_{31}$  harmonic was 400 times larger than the  $A_{11}$  and  $B_{11}$ , respectively. The profile produces small zonal harmonics with values about 300 times smaller than the target  $A_{31}$ , which indicates an effective control for the tested harmonics.

From the continuous magnetization-thickness map, it is possible to define the optimal shim shape. The shim shape is defined by the equally spaced contours that enclose areas with the same contour level.

Fig. 5 shows the continuous magnetization-thickness map, the valid domain, and the discrete shim profile to produce a harmonic  $A_{32}^{\text{target}} = -275$  ppm. The shim pattern is asymmetric with respect to the central plane  $Z = 0$  and corresponds to the asymmetry of the harmonic  $A_{32}$ . Fig. 5(g) depicts clearly a typical  $A_{32}$  spatial behavior. The figure of merit of this design was

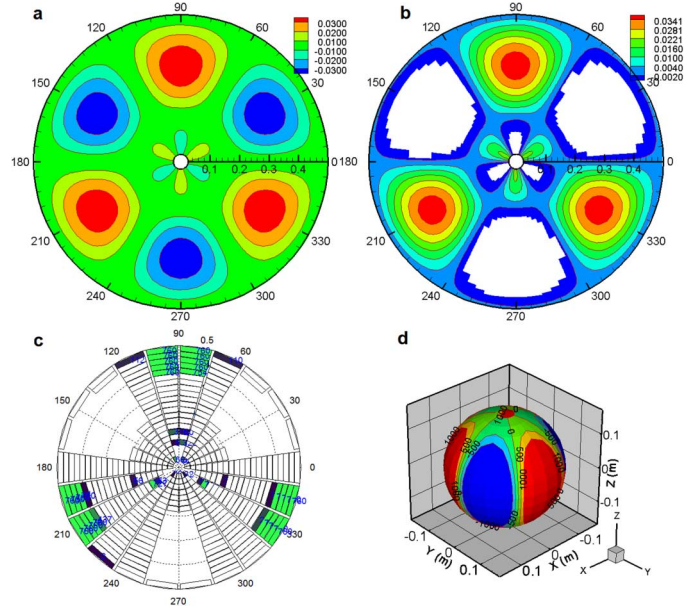


Fig. 6. Continuous magnetization-thickness map  $(S(\rho', \phi')/\max(\|S(\rho', \phi')\|) \cdot t)$  (a) and the valid domain for the discrete shim array (b). Discrete shim design to generate an  $B_{33}^{\text{target}} = -275$  ppm (c) with iron. The empty space in (b) shows the no valid domain. The magnetic field profile (d) generated by the discrete shim set (c) at the DSV. Units in (a,b) are given in meters and units in (d) are given in micro Tesla.

$\eta = 1.73 \cdot 10^{-5}$  T/(kg · ppm), 2.78 times larger than the  $\eta$  value produced by the conventional shim method. The profile shown in Fig. 5(e) and (f) generates a small  $B_{11}$  and  $B_{31}$  of values 100 and 182 times, respectively smaller than the target  $A_{32}^{\text{target}}$ . The remaining values of the harmonics  $A_{52}$ , is  $4.5 \cdot 10^3$  times smaller than the target value. The harmonic is generated with an error equivalent to  $-1.066$  ppm.

Fig. 6 shows the continuous magnetization-thickness map for generating a  $B_{33}^{\text{target}} = -275$  ppm. The difference between the target harmonic and the resulting harmonic was  $-0.45$  ppm. The figure of merit of this design was  $\eta = 2.2 \cdot 10^{-6}$  T/(kg · ppm), which is 1.8 times larger than the same parameter produced by the conventional shimming method. The profile depicted in Fig. 6(c), induces  $A_{20}$ ,  $A_{22}$ , and  $B_{11}$ . However, the influences in magnitude of the aforementioned harmonics, for all the cases, are more than 96 times smaller than the target  $B_{33}^{\text{target}}$ .

In this paper, we present only a part of all target harmonic evaluations performed with our approach. We realize that for a fixed harmonic order and target amplitude the figure of merit tends to decrease when the degree increases. For this reason, special attention is required for the selection of the number of orders and degrees to be compensated. If high degrees larger than  $m > 3$  are included in the target harmonic set, then a considerable amount of iron must be used to cancel the harmonic impurities thus requiring a large number of shim pieces to compensate the high frequency oscillations required by the target harmonics.

### B. Shimming a Combination of Harmonics

The present methodology was applied for a case where a combination of simulated harmonics forms part of the harmonic target set.

TABLE I  
TARGET HARMONICS SET

$A_{nm}^{\text{target}}$ (ppm)	(ppm)	(ppm)	(ppm)
$A_{10}=-100$	$A_{11}=100$		
$A_{20}=-90$	$A_{21}=0$	$A_{22}=0$	
$A_{30}=120$	$A_{31}=5$	$A_{32}=0$	$A_{33}=1$
$A_{40}=-275$	$A_{41}=0$	$A_{42}=0$	$A_{43}=0$
$B_{nm}^{\text{target}}$			
$B_{00}=0$			
$B_{10}=0$	$B_{11}=-30$		
$B_{20}=0$	$B_{21}=0$	$B_{22}=1$	
$B_{30}=0$	$B_{31}=0$	$B_{32}=0$	$B_{33}=-0.5$
$B_{40}=0$	$B_{41}=0$	$B_{42}=0$	$B_{43}=0$

The target harmonics shown in Table I, produces a peak-to-peak magnetic field inhomogeneity equivalent to 447.46 ppm. We have assigned zero ppm for some harmonics in order to demonstrate the ability of the approach to cancel target harmonics without introducing additional higher order terms. Fig. 7(a)–(g) shows the results obtained using this approach.

The addition of the unshimmed magnetic field and the magnetic field generated by the discrete shim array shown in Figs. 7(e), (f) reduces the peak-to-peak magnetic field inhomogeneity to 2.87 ppm. A minimal offset of  $0.06 \mu\text{T}$  was introduced in the main magnetic field  $B_0$ . The largest contaminant harmonic was  $B_{21}$ ; and its amplitude is more than 2 times smaller than the maximal shimmed harmonic value. See Table II. This means that the introduced contaminant value does not contribute significantly to the final field inhomogeneity. Contaminant harmonics are generated due to the rounding procedure used to produce integer proportions of the shim minimal thickness  $t_0$ . The introduced higher degrees corresponding to order four were 100–800 times smaller than maximal shimmed harmonic value. Therefore, using this method, the harmonics excluded in the target set are effectively controlled, while at the same time the target set is minimized. The figure of merit value corresponding to the discrete array was  $\eta = 7.96 \cdot 10^{-5} \text{ T}/(\text{kg} \cdot \text{ppm})$  and the weight of the iron shim set was 1.29 kg. Fig. 8 describes a ferroshim profile to correct the harmonic presented in Table I, considering the field contribution of all the shims uniformly distributed on the two pole faces. The figure of merit  $\eta = 3.30 \cdot 10^{-5} \text{ T}/(\text{kg} \cdot \text{ppm})$ , was 2.41 times smaller than the same parameter produced with our approach and the corrected peak-to-peak field inhomogeneity was 8.79 ppm using 1.4 kg of iron. The total shim set weight was about the same as that needed by a conventional approach (assuming the contribution of all shim pieces of unit strength source amplitude) but the homogeneity was improved by approximately a factor of three using the profile shown in Fig. 7(e) and (f). Comparing the shim pattern Fig. 7(e), (f) with Fig. 8(a), (b) we realize that using our approach the shim pieces are clustered at the border of the shim plate due to the constrained domain. The shims placed at this region reach the maximal thickness while the profile presented in Fig. 8(a) and (b) shows a spread thicknesses over the shim domain.

From the practical point of view, the profiles Fig. 7(e), (f) produces a significant advantage because the shimming work area is reduced and concentrated only in a well-defined region and therefore a minimal number of iterations is required.

### C. Magnetic Coupling Effect Over High Degree Harmonics

As mentioned before, the magnetic coupling is an effect that must be taken into account for an accurate thickness calculation.

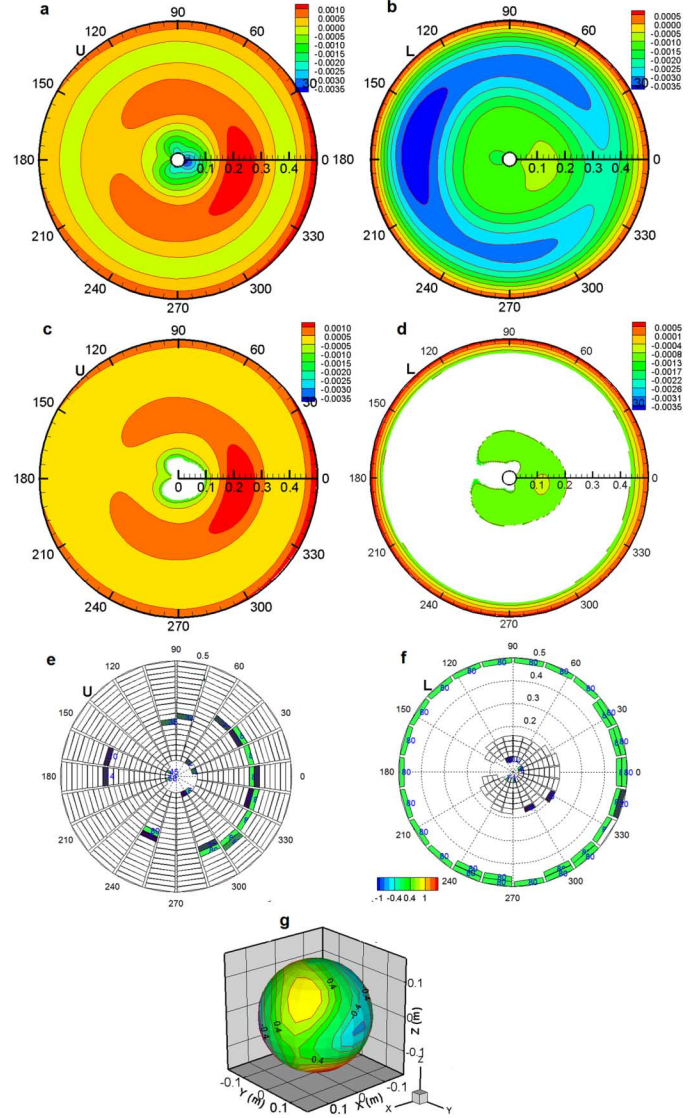


Fig. 7. Continuous magnetization-thickness map (a, b) for the pole faces (U and L) and the valid domain (c and d) for the discrete shim array (e and f). Combining the magnetic field generated by the discrete set (e and f) with the existing impurities shown in Table I, produces a corrected field homogeneity (g) equivalent to 2.87 ppm. The homogeneity showed in (g) is given in ppm. Units in (a,b,c,d) are given in meters.

TABLE II  
SHIMMED HARMONICS SET

$A_{nm}^{\text{shimmed}}$ (ppm)	(ppm)	(ppm)	(ppm)
$A_{10}=-5.5 \cdot 10^{-2}$	$A_{11}=-0.29$		
$A_{20}=0.79$	$A_{21}=-0.22$	$A_{22}=68 \cdot 10^{-4}$	
$A_{30}=-0.46$	$A_{31}=0.18$	$A_{32}=-0.041$	$A_{33}=-0.01$
$A_{40}=0.12$	$A_{41}=-35 \cdot 10^{-2}$	$A_{42}=-0.03$	$A_{43}=73 \cdot 10^{-4}$
$B_{nm}^{\text{shimmed}}$			
$B_{00}=0$			
$B_{10}=0$	$B_{11}=-0.44$		
$B_{20}=0$	$B_{21}=0.37$	$B_{22}=0.22$	
$B_{30}=0$	$B_{31}=-0.19$	$B_{32}=-2.8 \cdot 10^{-3}$	$B_{33}=-0.033$
$B_{40}=0$	$B_{41}=0.165$	$B_{42}=9.7 \cdot 10^{-3}$	$B_{43}=9 \cdot 10^{-4}$

The ferroshim set creates a reciprocal magnetic field influence among all iron pieces and hence a change of orders  $10^{-3} \text{ T}$  in the induced magnetization values are produced. For this reason

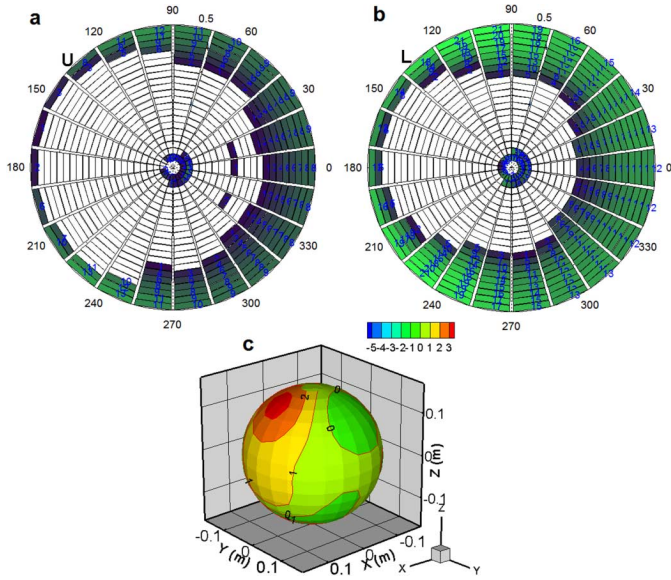


Fig. 8. Discrete shim array assuming the contribution of all iron pieces (conventional shimming approach). Upper shim domain (a) and lower shim domain (b). The shimmed homogeneity was 8.79 ppm. The homogeneity profile showed in (c) is given in ppm.

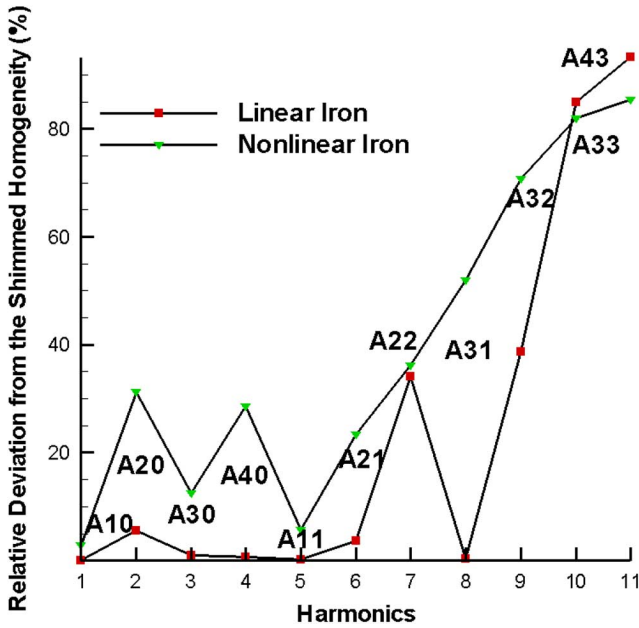


Fig. 9. Relative deviation of the shimmed inhomogeneity calculated with magnetic coupling respect to the same parameter neglecting the magnetic coupling. Linear and nonlinear iron was considered for the simulations.

an iterative process to update the shim thicknesses and the magnetization is required.

Fig. 9 shows the relative deviation of the shimmed inhomogeneity, assuming the magnetic coupling, from the same parameter produced by a discrete shim set neglecting the magnetic coupling.

We realize that when the magnetic coupling is not assumed in the magnetization calculus, a small effect over low orders and degrees is produced when the shimming is performed with linear iron. It means that only low orders can be canceled without a significant error over the final shim thicknesses and the target homogeneity. Neglecting magnetic coupling how-

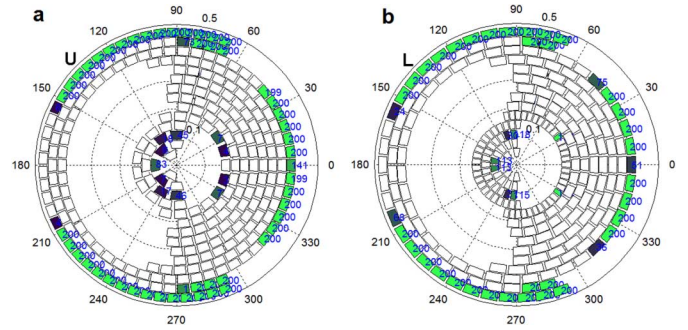


Fig. 10. Discrete shim array assuming the same size of the shim pieces (a) and a variation of design using the different shim sizes (b). The profile is designed to produce  $A_{31}^{\text{target}} = -275$  ppm.

ever, can induce large errors in the target homogeneity due to its influences over the higher degree harmonics. The same effect is created over the harmonics  $B_{nm}$ . Generally, the harmonics ( $A_{22}, A_{32}, A_{33}, B_{22}, B_{32}, B_{33}$ ) form part of the target set. Fig. 9 shows that magnetic coupling produces a higher impact over low and high order, and degrees when nonlinear iron is used for shimming the magnetic field.

#### D. Discrete Representation of the Shim Array

They are many ways to arrange the shim pieces to form the discrete array. Iron pieces of the same and/or different shapes and sizes can be combined to obtain the best shimmed homogeneity. The robustness of the solution will depend on the condition of the matrix that contains the contribution of each shim piece to the target harmonic set. This means that different combinations of shim sizes can produce more solutions that are less sensitive to rounding errors. Although, from a practical point of view, it is preferable to form the shim set with pieces of the same size. Fig. 10(a) shows a shim pattern to produce the harmonic  $A_{31}$  using a uniform shim size. The matrix condition number of this design is 397.3 and 249.1 for the shim set shown in Fig. 4(c). The magnetic field homogeneity produced by the design presented in Fig. 10(a) was 8.13 ppm after rounding. The same parameter generated by the design depicted in Fig. 4(c) was 1.82 ppm after rounding. The profile presented in Fig. 10(b) is an intermediate variation between Fig. 4(c) and Fig. 10(a). We used the same shim size for three different radii. The condition number of this design was 347.54 and the shimmed homogeneity 3.99 ppm. For magnetic field homogeneity evaluation we consider all the impurities generated by the shim set.

The design that uses small shim pieces at the pole face center produces a source matrix with a smaller condition number and hence better field homogeneity after round-off can be obtained. The profile variation presented in Fig. 10(b) can be an optimum tradeoff between robustness and performance.

The matrix condition can be used as selection criteria when different solutions that nearly produce the same target field are part of the solution set. The same numerical experiment can be extended to shimming horizontal magnets using nonuniform shim sizes close to the magnet DSV.

## IV. CONCLUSION

A new shim design method and shimming approach has been presented to correct magnetic fields generated by open-type bi-

planar magnets for MRI. The magnetization-thickness function is expressed as a sum of orthogonal functions over the pole face dimensions, providing a useful map for shim topology. The weight of the total ferroschim set is minimized in the optimization process. The shim profiles produced by this approach generate harmonics with minimal impurities and both high order harmonics and the  $B_0$  offsets are effectively controlled. By restricting the possible placements of the iron pieces, it is possible to generate a better conditioned source matrix compared to unrestricted methods. The magnetic coupling effect produces a small impact over the low order harmonics but a very high impact over high order and degrees when linear iron is used for shimming. Taking both the nonlinearity of iron and magnetic coupling into account is very important to be able to obtain optimal results. The appropriate size selection and distribution of the ferroschim piece improves the condition of the source matrix; thus, robust solutions with minimal introduced impurities are obtained.

#### ACKNOWLEDGMENT

This work was supported by the Australian Research Council.

#### REFERENCES

- [1] D. A. Fishbain, M. Goldberg, E. Labbé, D. Zacher, R. Steele-Rosomoff, and H. Rosomoff, "Long-term claustrophobia following magnetic resonance imaging," *Amer. J. Psych.*, vol. 145, pp. 1038–1039, 1988.
- [2] M. G. Abele, W. Tsui, and H. Rusinek, "Methodology of pole piece design in permanent magnets," *J. Appl. Phys.*, vol. 99, pp. 08D903-1–08D903-3, 2006.
- [3] A. Trequatrini, S. Besio, S. Pittaluga, V. Punzo, and L. Satragno, "A novel 0.25 T dedicated MRI apparatus," *IEEE Trans. Appl. Supercond.*, vol. 16, no. 2, pp. 1505–1508, Jun. 2006.
- [4] Y. Yao, Y. Fang, C. S. Koh, and G. Ni, "A new design method for completely open architecture permanent magnet for MRI," *IEEE Trans. Magn.*, vol. 41, no. 5, pp. 1504–1507, May 2005.
- [5] R. Lemdiasov, R. Ludwig, M. Brevard, and C. Ferris, "Design and implementation of a uniplanar gradient field coil for magnetic resonance imaging," *Concepts Magn. Reson.*, vol. 20B, pp. 17–29, 2004.
- [6] H. Zhao, S. Crozier, and D. M. Doddrell, "Asymmetric MRI magnet design using a hybrid numerical method," *J. Magn. Reson.*, vol. 141, no. 2, pp. 340–346, Dec. 1999.
- [7] F. Romeo and D. I. Hoult, "Magnet field profiling: Analysis and correcting coil design," *Magn. Reson. Med.*, vol. 1, pp. 44–65, 1984.
- [8] L. K. Forbes, M. A. Brideson, and C. S. Crozier, "A target-field method to design circular biplanar coils for asymmetric shim and gradient fields," *IEEE Trans. Magn.*, vol. 41, no. 6, pp. 2134–2144, Jun. 2005.
- [9] M. A. Brideson, L. K. Forbes, and C. S. , "Winding patterns for biplanar MRI shim coils with rectangular and circular target-field regions," *Meas. Sci. Technol.*, vol. 15, pp. 1019–1025, May 2004.
- [10] M. A. Brideson, L. K. Forbes, and S. Crozier, "Determining complicated winding patterns for shim coils using stream functions and the target-field method," *Concepts Magn. Reson.*, vol. 14, no. 1, pp. 9–18, 2002.
- [11] J. V. M. McGinley, V. C. Srivastava, and G. D. DeMeester, "Passive shimming technique for MRI magnets," U.S. Patent 5 532 597, 1996.
- [12] G. Neuberth, "Integral passive shim system for a magnetic resonance apparatus," U.S. Patent 6 897 750, 2005.
- [13] B. Dorri, M. E. Vermilyea, and W. E. Toffolo, "Passive shimming of MR magnets: Algorithm, hardware, and results," *IEEE Trans. Appl. Supercond.*, vol. 3, no. 1, pp. 254–257, Mar. 1993.
- [14] H. Sanchez, F. Liu, A. Trakic, and S. Crozier, "A magnetization mapping approach for passive shim design in MRI," presented at the 28th Annu. IEEE Eng. Medicine Biol. Soc., New York, 2006.
- [15] L. K. Forbes and S. Crozier, "Novel target-field method for designing shielded biplanar shim and gradient coils," *IEEE Trans. Magn.*, vol. 40, no. 1, pp. 1–10, Jan. 2004.
- [16] C. Juchem, B. Muller-Bierl, F. Schick, N. K. Logothetis, and J. Pfeuffer, "Combined passive and active shimming for in vivo MR spectroscopy at high magnetic fields," *J. Magn. Reson.*, vol. 183, pp. 297–308, 2006.
- [17] R. Vadovic, "Magnetic field correction using magnetized shims," *IEEE Trans. Magn.*, vol. 25, no. 4, pp. 3133–3139, Jul. 1989.
- [18] J. S. Ryu, Y. Yao, C. S. Koh, and Y. J. Shin, "3D optimal shape design of pole piece in permanent magnet MRI using parameterized nonlinear design sensitivity analysis," *IEEE Trans. Magn.*, vol. 42, no. 4, pp. 1351–1354, Apr. 2006.
- [19] D.-H. Kim, B.-S. Kim, J.-H. Lee, W.-S. Nah, and I.-H. Park, "3D optimal shape design of ferromagnetic pole in MRI magnet of open permanent-magnet type," *IEEE Trans. Appl. Supercond.*, vol. 12, no. 1, pp. 1467–1470, Mar. 2002.
- [20] A. Podolskii, "Development of permanent magnet assembly for MRI devices," *IEEE Trans. Magn.*, vol. 34, no. 1, pp. 248–252, Jan. 1998.
- [21] L. Hong and D. Zu, "Shimming permanent magnet of MRI scanner," presented at the PIERS China, 2007.
- [22] Y. Zhang, D. Xie, and P. Xia, "Passive shimming and shape optimization of an unconventional permanent magnet for MRI," *IEEE Trans. Magn.*, vol. 32, pp. 2640–2642, 1996.
- [23] T. Matsuda, A. Ariyoshi, and H. Tanabe, "Field corrections of open MRI superconducting magnets," *IEEJ Trans Ind. Applicat.*, vol. 125, pp. 774–778, 2005.
- [24] X. Bu-Xin, M. Mruzek, P. Eckels, W.-X. Wang, and Y. Tan, "An open refrigerator cooled superconducting magnet for the special purpose of magnetic resonance imaging," *IEEE Trans. Magn.*, vol. 32, pp. 2640–2642, 1996.
- [25] X. Huang and B. C. Amm, "Method and apparatus for passive shimming of magnets," U.S. Patent 6 778 054 B1, 2004, GE company.
- [26] S. Kakugawa, N. Hino, A. Komura, M. Kitamura, H. Takeshima, T. Yatsuo, and H. Tazaki, "Three-dimensional optimization of correction iron pieces for open high field MRI system," *IEEE Trans. Appl. Supercond.*, vol. 14, no. 2, pp. 1624–1627, Jun. 2004.
- [27] C. D. Eccles, S. Crozier, M. Westphal, and D. M. Doddrell, "Temporal spherical harmonic expansion and compensation of eddy-current fields produced by gradient pulses," *J. Magn. Reson. A.*, vol. 103, pp. 135–141, 1993.
- [28] A. Canova and M. Repetto, "Integral solution of nonlinear magnetostatic field problems," *IEEE Trans. Magn.*, vol. 37, no. 3, pp. 1070–1077, May 2001.

Manuscript received September 25, 2007; revised December 12, 2007. Corresponding author: H. Sanchez Lopez (e-mail: hsanchez@itee.uq.edu.au).